Enhancing Controller Efficiency in Hybrid Power System Using Interval Type 3 Fuzzy Controller with Bacterial Foraging Optimization Algorithm

J. VINOTHKUMAR[1*], R. THAMIZHSELVAN[2]
[1]Department of Electrical Engineering, Annamalai University, Annamalai Nagar, Chidambaram, Tamil Nadu 608002, INDIA
[2]Department of Electrical Engineering, Annamalai University, Annamalai Nagar, Chidambaram, Tamil Nadu 608002, INDIA

Abstract: Microgrids (MGs) are designed with the help of effective power extracted from renewable sources such as rooftop solar panels, photovoltaic cells, batteries, floating PV and solar PV with the grid. In a hybrid microgrid, Interlinking Converter (ILC) is a key component to connect the AC sub-grid and DC sub-grid. DC-DC converters are being used as power converters in between load and source to enforce and increase the PV depending on the voltage output signal. Accordingly, the work focused on a Multi-Input (MI) KY boost converter. This Proposed topology gathered maximum power using multi-input KY boost converters for hybrid energy. This hybrid topology operates mainly delivered power from renewable energy sources solar/wind to dc bus. In the absence of any one source, wind or solar supplies power to the dc bus. Without any renewable energy, sources battery deliver the power to the dc bus. The research proposed the interval type 3 fuzzy controller is used for controlling the load frequency of the multi-area system. Swarm-based hybrid metaheuristic optimizer of the Bacterial Foraging Optimization Algorithm (BFOA) is proposed for optimal tuning and controlling the PI controller parameters. Controlling the reactive power of the hybrid power system model with the aid of a Static Synchronous Compensator (STATCOM). A unique controller is deployed to regulate the AC and DC currents of the STATCOM using two PI controllers. In this paper effectiveness of the hybrid power system is simulated through MATLAB/SIMULINK. The battery current and voltage of this produce 2000 A and 205 V, grid voltage produced in this work is 1.9×10^4 V and the power of the work produce approximately 90 kW. The results show that the interlink converter improves the flexibility of the hybrid microgrid and, in addition, the power quality of the energy supplied in the utility grid is improved. In future, an intelligent control algorithm may be presented to improve the control strategies of the HMG, respectively.

Keywords: Microgrids, Hybrid Metaheuristic Optimizer, Interlinking Converter, Fuzzy Controller, Multi-Input KY Boost Converter, and STATCOM.

Received: September 18, 2022. Revised: May 21, 2023. Accepted: June 16, 2023. Published: July 17, 2023.

1. Introduction

To meet the significant rise in electrical energy demand and address the pollution issues brought on by the use of fossil fuels, the integration of renewable energy sources (RESs) into electrical systems has become a required and crucial concern. Electricity is produced using a variety of RESs, such as wind, photovoltaic (PV), fuel cells, and biomass. According to the annual growth rate of RESs, wind and solar power are the two RESs that are most frequently included in electrical systems because of their numerous benefits [1-2]. The best way to establish microgrids is by using renewable energy, especially in islands and autonomous regions where they can be placed close to areas of demand, reducing the cost of installing conventional power grids. Systems for generating renewable energy might be either grid-connected or island utilities. The problem of the

indiscriminate character of renewable energy resources, where these sources rely on unexpected weather conditions that did not have the full accuracy required to produce energy, is typically overcome by the use of more than one energy source [3]. In a lot of industry research, controllers are commonly used. This aids in eliciting the necessary answers from the various types of controllers being employed in research. Three different types of inverter controllers are frequently employed in the current study. When an automatic controller is required to control a process, Proportional Integral (PI) control is a sort of classic control that is frequently employed in the industry. An accurate mathematical model of the system is required by the PI controller used in wind turbine pitch control systems. Here, the pitch angle controller is optimised using a novel applicable optimization approach [4]. Adaptive control is the term used to describe the discontinuous control method known as sliding mode control (SMC). It is a reliable control technique. SMC preserves trajectories on the sliding surface and changing structure and is composed of similar control [5-6].

There is excess power available when generation is greater than the load required, typically during the busiest weather conditions. Storage units store the energy at this time for a brief period. When the amount of energy generated falls short of the increase in load demand, this stored energy is put to use. Integration in the environment of fractional order (FO) calculus for proportional-integral-derivative (PID) controller and fuzzy controller, referred to as FO-Fuzzy PID controller tuned with the quasi-opposition-based harmonic search algorithm, has been proposed [7] to control the deviation in frequency and power. To achieve great efficiency, the intelligent multi-input multi-output fuzzy controller has been presented [8]. Even though these systems demonstrated superior performance, it might still be raised by using a potent optimization strategy. A PID controller is used in the system under study, and the technique of moth flame optimization is used to adjust its parameters [9]. A unique approach based on the fusion of the harmony search algorithm and the fuzzy logic controller is proposed in [10]. This technique, which is based on environmental data, will determine the ideal size of a hybrid energy system (load demand, solar irradiation, and wind speed). Hybrid Wind-Solar Energy Systems, which combine wind and solar energy generating, have been used in recent years to address the intermittent nature of renewable energy generation units. To increase the maximum power tracking efficiency of grid-connected wind and PV coupled to the back-to-back converter DC link. The Grid Side Converter and Rotor Side Converter are controlled using Stator Flux-Oriented control [11]. Power converters that connect the AC and DC sub-grids in the hybrid microgrid are used for the interfacing of these grids, which is essential for ensuring the stability of the entire microgrid. To measure the power demand of the AC and DC sub-grids in line with terminal AC bus frequency and terminal DC bus voltage, respectively, a bidirectional droop control approach for the converter is presented. Additionally, it establishes the amplitude and direction of the power transmission through the converter [12].

To maintain a power balance in a hybrid microgrid while taking the source and load variation into consideration, an iterative learning controller is presented [13]. To maintain constant dc bus voltage, the primary or local level control is used with solar and batteries. To deliver stable voltage, ensure smooth grid synchronisation, and ensure proper real power sharing across dc/ac buses, the secondary or system level control is achieved by managing the interlinking converter situated between the ac and dc bus. Each component of the proposed system is optimised by utilising experimental design methodologies based on the most affecting parameters to attain

the best performance and efficiency [14]. A reliable and improved load frequency control (LFC) approach is necessary for the power system to run smoothly in the aftermath of RESs intermittency and continuously changing load demands. So, to deal with the frequency abnormality brought on by the existence of renewable producing units in the current power system, a cascade fuzzy non-integer FO-PID control policy is developed [15]. In a hybrid microgrid, an interlinking converter (ILC) is a key component to connect the AC subgrid and DC subgrid. Its control strategy significantly affects power flow management, power quality, system efficiency and stability. Traditionally, ILC is usually controlled as a current source, resulting in poor dynamic stability when a remote weak AC subgrid is connected by a large linking impedance. The remaining part of the work is organized as follows, section 2 portrays the literature survey of the study, and the research problem definition and motivation are exposed in section 3. The proposed research methodology is disclosed in section 4, section 5 elucidates the experimentation and result discussion section, and section 6 reveals the conclusion of the research work.

2. Literature Survey

Globally, RES-based hybrid power systems are being used more and more to cut carbon emissions. However, RESs are sporadic and incredibly unpredictable, which can lead to significant frequency variations. By using controllers that are ideally built, these fluctuations can be kept within the appropriate limits. An LFC structure based on a tilt fraction-order integral (TI) controller and an FO-PID controller with a filter was proposed by Ahmed *et al* [16]. Artificial Gorilla Troops Optimizer is used to create this proposed controller in the best possible way. The impact of the large penetration of renewable is also investigated on the considered power system with the proposed controller. The performance of the system is improved in [17] using the recently created improved squirrel search algorithm (ISSA), which is utilised to adjust the parameters of several controllers, including the PID, two- and three-degree PIDs, as well as cascaded 2DOF-PID fractional order integrals (FOI). The performance of the optimal controller was modified using integrated Particle Swarm Optimization (PSO) and Squirrel Search Algorithm (SSA). Numerous case studies have been created to evaluate the system's reliability, adaptability, and flexibility.

In [18], a hybrid power system is employed, which includes a thermal system, wind, solar, diesel engine generators, electric vehicles, and energy storage systems such as batteries and superconducting magnetic energy storage. The frequency has been controlled via a reliable FOPI frequency controller. The Water Cycle Algorithm optimizes the FOPI parameters. The objective function chosen is the Integral Time Absolute Error (ITAE). The results of the proposed algorithm are compared with those of PSO, another well-known optimization technique, to demonstrate its effectiveness. By maintaining a faster settling time, the suggested optimization method performs better than the PSO. To address the frequency anomaly caused by the existence of renewable generating units in [19], a cascade fuzzy-noninteger FO with proportional derivative with filter-proportional integral (CFPDF-PI) control policy is suggested. FPD-F is used as the master and integer-order PI is used as the slave in the CFPD-F-PI controller. To fine-tune the controller parameters, the recently developed slime mould algorithm is used as a stochastic optimizer. The proposed approach's ability in LFC and adaptability for other real-world applications are validated by various scenarios for the robustness study.

To enhance the operation of Microgrids (MG), increase system reliability, and increase effective efficiency, which is a vital characteristic, a new hybrid model is

presented [20]. FLC-based EMS with AC/DC microgrid implementation is done. The power quality of the MG is increased in addition to the EMS design. It suggests analysing and managing storage devices. The FLC extends battery life and produces an ideal SoC. To reduce power quality problems caused by nonlinear, unbalanced load conditions, an FLC-based EMS grid-integrated MG is implemented. For automatic load frequency management (ALFC) of a hybrid power system, a chaotic search-based hybrid Sperm Swarm Optimized-Gravitational Search Algorithm is presented in [21]. The integral time absolute error of the hybrid system is minimized to produce the control parameters of the PID controller for ALFC, which controls the system's frequency. With various power source combinations linked to the system, the effectiveness of the suggested technique is tested. Additionally, a sensitivity analysis is conducted to examine the suggested technique's flexibility while taking into account RES's real-time weather intermittency and load change.

In [22], the innovative Fuzzy-PID+PID hybrid controller that is employed for frequency regulation in a hybrid power system is optimised using the whale optimization algorithm (WOA). At the time, the suggested application of the WOA approach for frequency regulation in HPS may be considered unique. When compared to other controllers, the suggested WOA optimised Fuzzy-PID + PID hybrid controller performs at the highest level, demonstrating the effectiveness of WOA in load frequency control experiments. Due to the nature of the spatial and temporal variability connected with renewable energy resources and the large operation uncertainties brought on by the changing natural environment, the long-term optimal operation of RES is a difficult challenge. For the long-term operations of the RESs, the stochastic model predictive control (MPC) is conceived and implemented based on probabilistic forecasting and rolling stochastic optimization [24]. PV energy generation systems have been rated as a top energy system by power suppliers all over the world due to the use of RES to create electricity. These energy options have the drawback of being unpredictable and dependent on climate and weather conditions. To execute noise-free voltage stress reduction for DFIG and PV systems, an effective strategy utilising a landsman converter is designed [25]. The maximal power tracking point is controlled using a PWM-based PI controller that uses the firefly method. A grid-synchronized 3-phase VSI with an LC filter inverts the DC voltage to AC while assuring smooth operation and eliminating harmonics. The outputs showed a minimum THD value of 1.8%.

3. Research Problem Definition and Motivation

Today, the need to generate electricity from clean and green resources has become a necessity. Classic thermal power plants, due to the use of fossil fuels, have polluted the environment and destroyed many natural resources. These serious concerns have led researchers, policymakers, and investors in energy to research and develop power generation microgrids that reduce dependence on fossil fuels and reduce environmental impacts. Although these resources have many benefits and are sustainable, clean, and inexhaustible, they have low efficiency because they have significant limitations, such as variable solar irradiance and fluctuating wind speed. A combination of more than one resource for power generation systems from renewable energy resources or hybrid renewable energy systems (HRES) is used to overcome this problem. Furthermore, to address this problem, it is necessary to develop appropriate energy storage systems for the HRES. Among the renewable energy sources, biodiesel, a clean diesel fuel producible renewable natural resources, wind turbines (WTs) and photovoltaic (PV) systems are often

considered the most promising technologies to meet electrical loads in rural or remote regions. The use of different renewable energy sources in supplying power to HRESs increases the reliability of the power generation system and, consequently, requires fewer support units; in other words, the ability to supply power to the consuming power system increases during the year.

The impact on the stability of power systems is rising as the penetration level of renewable energy with sporadic natures rises rapidly on the grid. Transient stability is the property of a power system to regain its normal operating condition following sudden and severe faults in the system. The transient stability study is extremely important for maintaining the continuity of the power flow and properly controlling modern electrical power systems with multiple renewable energy sources integrated into them. Some of the mentioned FCLs and other auxiliary means of enhancing stability incur additional costs due to the use of converters, coupling transformers, and filters. It is important to investigate a cost-effective and new method for transient stability improvement of hybrid power systems. The existing research has not studied the system characteristics of the AC-DC hybrid grid when it is integrated with a large number of renewable energy technologies, and the mutual coupling between DC and renewable energy has not been considered when evaluating the renewable energy penetration capacity of the power grid. Therefore, the renewable energy penetration capacity evaluation results are not fully applicable to the AC-DC hybrid grid.

4. Proposed Research Methodology

In recent years, smart grids and microgrids are becoming important topics for energy demand. The microgrid paves a way to effectively integrate various sources of distributed generation (DG), especially renewable energy sources, and thus reduce CO_2 emissions. However, it must be considered that increasing levels of penetration of DGs may cause severe phase voltage imbalance, resulting in a larger ground current and descending power quality. An improved fuzzy-based energy management strategy is proposed for a hybrid power system with multiple power sources consisting of Rooftop solar panels/photovoltaic cells (PV)/battery (BAT)/floating PV/ solar PV with the grid. The power demand from the propeller and user terminal is afforded by the power sources connecting to power converters. The high and stable power satisfies the power demand even under extreme work conditions. Figure 1 illustrates the flow diagram of the proposed work.

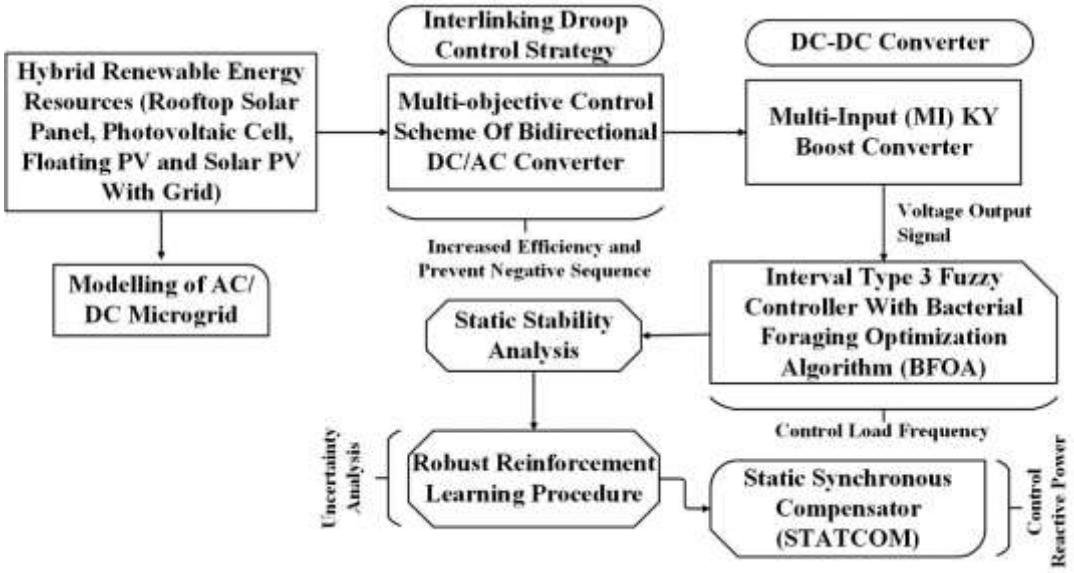

Figure 1: Flow Diagram of the Proposed Work

Nowadays, the power system dynamics have been considerably influenced because of the growing renewable power penetrations. A microgrid is a small-scale electrical system composed of distributed generation (DG) and energy storage devices (ESD) technologies, with the aiming to meet the demand of local loads. These devices, acting together, allow the microgrid to operate in both connected and standalone modes. Such aspects increase the system's versatility and power flow possibilities, which improve the efficiency, reliability, and quality of the energy supplied. According to the sources and loads connected to them, the microgrids can be classified as AC microgrid, DC microgrid, and hybrid AC/DC microgrid.

4.1 Modelling of AC/DC Microgrid

Microgrids have become an attractive option for distributed generation (DG) with the increase in Renewable Energy Sources (RES) and storage systems. Microgrids (MGs) are designed with the help of effective power extracted from renewable sources such as Rooftop solar panels, Photovoltaic cells, batteries, floating PV and solar PV with the grid. Furthermore, particularly when paired with renewable generators, batteries help provide reliable and cheaper electricity in isolated grids and off-grid communities. Lithium-ion batteries were chosen for this study due to their high energy density, long life cycle, and high efficiency. The existence of both AC and DC microgrids has led to a new concept of hybrid AC/DC microgrids which consists of both AC and DC grids tied by an Interlinking Converter (ILC).

Rooftop Solar Power Plant: Appropriate sizing of the rooftop PV system in terms of the number of PV panels and the sizing of the battery are important aspects of the design. In this section, we present a mathematical model, in which we develop the expressions for sizing and the number of solar panels and batteries as a function of load requirement. The model includes both technical and economic analysis.

Photovoltaic Cells: Solar Photovoltaic (PV) cells generate electricity by absorbing sunlight and using that light energy to create an electrical current. There are many PV cells within a single solar panel, and the current created by all of the cells together adds up to enough electricity to help power your school, home and businesses.

Floating PV System: A developed PV floating power generation results from the combination of PV plant technology and

floating technology. This fusion is a new concept for technology development. As a new generation technology, it can replace the existing PV plants that are installed on top of woodland, farmland and buildings. The PV floating plant consists of a floating system, mooring system, PV system and underwater cables.

Grid-Connected Photovoltaic System: Grid-connected solar PV (GCPV) systems, floating PV, rooftop PV, and PV cells include building integrated PV (BIPV) systems and terrestrial PV (TPV) systems. TPV systems include plants in deserts and tides. Analysis of optimal photovoltaic (PV) array and inverter sizes for a grid-connected PV system. The inverters and DC-DC converters or DC-AC converters are used for power conversion. However, hybrid AC/DC microgrids are presented in the following section.

4.1.1 Hybrid AC/DC Microgrid Description

The hybrid AC/DC microgrid topology studied in this paper comprises distributed generation, electrical loads, an energy storage device, and the utility grid. Each one of these elements is detailed in the following subsections.

Distributed Generation

The DG of the microgrid is composed of RES, such as photovoltaic and wind generation. These primary sources behave according to the profile of solar irradiation and wind speed. The electric current generated by the RES does not meet the voltage and frequency requirements of the power grid; thus, power electronic converters are employed to interface the connection between the DG and the microgrid. Such converters can be represented by a current source. In the analyzed hybrid microgrid, the photovoltaic and the wind generation are defined as a DC source and AC source, respectively, as detailed hereafter.

DC Source: The DC source represents a set of photovoltaic modules connected to a DC-DC converter operating with Maximum Power Point Tracking (MPPT). To simplify the analyses, such a system is approximated by an ideal current source injecting power into the microgrid's DC side.

AC Source: Wind generation is an example of RES as an AC source. In general, these systems consist of a wind turbine associated with a back-to-back converter, which allows injecting the power generated into the utility grid. In a simplified way, the wind system is represented by a controlled three-phase AC source connected to the AC microgrid.

Loads

DC Load: Devices that consume direct currents, such as DC machines, electric vehicles, and many electronic devices, are defined as DC loads. Similarly to the DC source, the DC load is represented as a controlled direct current source, but functions by absorbing power from the microgrid.

AC Load: The AC loads are represented by sets of impedance, composed of balanced three-phase resistors and inductances in series. Thus, these AC loads consume the active and reactive power of the AC microgrids (ACMG). The input and output of such loads occur according to the desired power profiles.

Nonlinear Load: The nonlinear load represents devices that distort the electrical current waveform, contaminating the grid with harmonic content. Such loads are modelled as a diode rectifier bridge with a resistive load and inductive filter at the input. The distortion in the waveform occurs due to the harmonic components added to the fundamental sinusoidal current. These harmonic distortions cause issues in the utility grid, thereby affecting the power quality of the energy supplied by the system.

Energy Storage Device

Among different existing energy storage technologies, Li-ion batteries are chosen as ESD in this work. The dynamic behaviour of such ESD is based on the Shepherd model, which represents the battery as a controlled DC source in series with internal resistance.

It is possible to describe, in a simplified way, the output voltage of the battery bank, according to equation (1).

$$V_{bat} = E_{bat} - R_{bat} I_{bat} \quad (1)$$

Where, V_{bat} and E_{bat} are the output and internal battery voltage, respectively; R_{bat} is the internal resistance, and I_{bat} is the battery's electrical current.

Utility Grid

Despite the main aspect of a microgrid being the possibility of operating in the standalone or grid-connected mode, this paper focuses exclusively on studying the grid-connected operation. In this study, the utility grid is implemented by a balanced, 60 Hz, three-phase, 220 V RMS, phase-to-phase AC source. Each voltage source represents a phase, with 120º of phase-shift between each phase, in the positive sequence. RL impedances are employed to characterize the conductors' dynamic effect, emulating the transmission line impedances. The value of these impedances is determined according to conventional short-circuit power for electrical distribution systems.

ILC Control

The ILC is the device that connects and promotes the bidirectional power flow between the DCMG and ACMG. The main function of such a converter is to form the DCMG and perform the power-sharing inside the HMG. Two control loops are employed to drive the ILC. The internal loop controls the current in the L filter, while the outer loop controls the voltage on the DC-link capacitors.

From the active and reactive power references, the current references are established for dq axis, respectively, as:

$$I_{d_{REF}} = \frac{2}{3}\frac{P_{REF}}{V_d} \quad (2)$$

$$I_{q_{REF}} = -\frac{2}{3}\frac{Q_{REF}}{V_d} \quad (3)$$

Where, $I_{d_{REF}}$ and $I_{q_{REF}}$ are the current references dq axis, respectively; P_{REF} and Q_{REF} are the active and reactive power references, respectively. These equations are the same for both ILC and VSC_a devices.

The PI controllers employed on the ILC are designed by frequency response by setting the crossing frequency and the phase margin. The ILC control strategy has the objective to compensate the reactive power into the utility grid and apply a power-sharing by droop technique.

4.2 Converter

In a hybrid microgrid, Interlinking Converter (ILC) is a key component to connect the AC subgrid and DC subgrid. Its control strategy significantly affects power flow management, power quality, system efficiency and stability. It comprises a DC grid and an AC grid interlinked by a multi-objective control scheme of a bidirectional DC/AC converter. Such a hybrid AC/DC microgrid has the advantages of both AC and DC with increased efficiency and less cost. The primary or local level control is implemented for solar and battery for maintaining stable dc bus voltage. DC-DC converters are being used as power converters in between load and source to enforce and increase the PV depending on the voltage output signal. Further, the work is focused to build a new boost converter of Multi-Input (MI) KY boost converter. The secondary or system level control is implemented by controlling the interlinking converter placed between ac and dc buses to supply stable voltage along with the smooth grid synchronization and ensuring the proper real power sharing between dc/ac buses. Additionally, the ILC control prevents any negative sequence currents from entering the AC source.

4.2.1 Multi-Objectives Control Framework

In this section, a study about the design of the proposed two-stage control framework is exposed for the stable and voltage-tracking operation of the HMG over the variable generation and load changes. For the reliable operation of the HMG, the following points need to be met leastwise while designing the control framework.

Maintain stable DC bus voltage for the variation of temperature and irradiance.

- Require to incorporate the precise converter control model to assist the DC bus bar in reaching fast transient performance against the varying generation conditions.
- Control the inverter accurately associated with the load network to minimize the mismatch voltage with the corresponding reference voltage set by the consumer.
- Implement a robust control method in the inverter associated with the load network to deal with high performance over the external uncertainties produced due to changes in load dynamics.
- To require a synchronised operation between the AC and DC side of the HMGs so as proper power sharing among the primary grid and DC side can be made.

The design process of the proposed controller has been divided into two stages to deal with multiple objectives over the above-mentioned challenges. The first control stage designed via the partial feedback linearization method addresses the first pair of mentioned challenges, whereas the second stage deals with the next two pairs. Additionally, a VSC controlled by the PI controller is implemented to maintain the operational synchronization between the DC side and AC side of the HMG.

4.2.2 Bidirectional DC–AC Converter Topology

To validate the fuzzy logic-based control technique implemented in this proposed HMG, we had to design a bidirectional DC–AC converter that was capable of functioning as both an inverter and a PFC rectifier. The transition between these two modes of operation needed to be fully automated and without human intervention for our HMG to autonomously store, produce and supply energy for domestic use.

Before validating its operation by appropriate experimental measurements, it is essential to detail the operating modes of the converter, as well as its control strategies.

Proposed Topology and Details of Its Operating Modes

The energy transfer between a DC voltage source and an AC voltage source, and vice versa, was the basis of this structure. The association in series of a DC–DC stage and a DC–AC stage ensured this principle of operation with these two stages being necessarily bidirectional.

The DC–DC stage needed to generate a rectified sine wave from the PWM command of the power switches. Since the power devices in this stage switched at a frequency of a few hundred kilohertz to optimize the compactness of the whole converter, the inductance, noted L1 was sized so that the ripple of the current was negligible compared to the sinusoidal component at low frequency (in this case, 50 Hz). Therefore, the DC–DC converter acted as a controllable output voltage source.

By changing the voltage of a modulation stage, the output current could be regulated. This is very interesting, especially when the output current is strongly reduced or in the of variable DC voltage. This strategy allowed the output voltage of the DC–DC stage to be modulated. Specifically, when this modulated voltage was higher than the mains voltage, the output current had a positive value. In the opposite case, the output current was negative.

The design approach that was chosen allowed the converter to be used in both grid-connected and off-grid modes. Since

the microcontroller was synchronized with the AC grid to sensibly drive the DC–DC and DC–AC stages, only the grid-connected mode will be discussed in the remainder of this paper.

The DC–AC stage was responsible for inverting every other sinusoidal half-wave to obtain a full sinusoidal output signal.

Compared to existing voltage source converter topologies, such as multilevel structures, the coupling of a DC–DC stage with an H-bridge has many advantages:

- The standard DC–DC converter and the H-bridge are two very common and mastered topologies;
- Many H-bridge topologies are composed of four or more power components that switch at high frequencies. In our proposed architecture, only those in the DC–DC stage (see transistors $T1$ and $T2$) operated at high frequency, i.e., 150 kHz implemented here. In the DC–AC stage, all components (see components $T3$, $T4$, $T5$ and $T6$) switched at low frequency, i.e., 50 Hz;
- When switching at high frequency, it is imperative to take into account the delay between the two switching operations in the same branch for safety reasons. Here, the safety delay was easier to regulate since only one stage operated at high frequency;
- In our architecture, the capacitance used at high frequency to modulate the voltage Vc was small (about 10 µF).

Control Strategies

In this section of the paper, we will describe the control strategies of the proposed bidirectional DC–AC converter. We will only give the principles and thus, we will not detail the control circuit or the AC network connection strategy because several patents are pending.

The DC–AC stage was controlled by the very same signal as the inverter mode, so it was synchronized with the AC grid at a switching frequency of 50 Hz

4.2.3 Multi-Input (MI) KY Boost Converter

As shown in figure 2 (a), a multi-input converter is a circuit structure that integrates different input voltage sources with different voltage levels and supplies an output dc load. According to the principles of circuits and systems, a syncretization of dc-dc converters depends on whether it consists of a pulsating current source or pulsating voltage source. In the case of pulsating current sources such as boost converters, these modules need to be connected in parallel to supply the load. Figure 2 (a) and figure 2(b) respectively show this principle and a circuit example in boost converters.

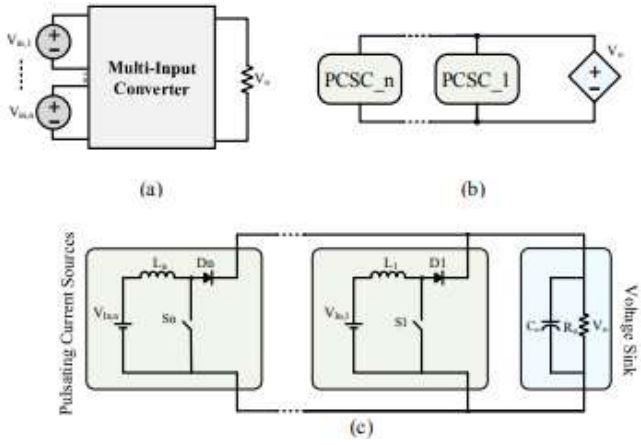

Figure 2: Derivation of Multi-Input DC-DC Converters

The main part of the proposed system is the multi-input KY boost dc–dc converter that is linked to two renewable energy sources. DC–DC KY boost converter connected between energy sources and the dc bus. Multi-input KY boost converter system architecture of a solar array system/wind system. The maximum power point (MPP) tracking of both renewable energy sources, is accomplished with two controllable switches. The integration of a synchronously rectified boost converter, a KY converter and coupled inductor, modified KY boost converter is presented here. The coupling inductor improves the voltage gain.

The corresponding voltage gain can be expressed as:

$$\frac{V_{out}}{V_{in}} = \frac{1+(k-1)D}{1-D} \quad (4)$$

Where, $K = Ns/Np$

In this paper, the design parameters are the inductance and capacitance are chosen as $Lin = Lo = 1mH$, $C1 = C2 = 200\,uF$ and A $Co = 3300\,uF$. $Vin = 270V$, $Vo = 640V$, the voltage conversion ratio is set at $K = 300/20 = 15$, frequency 100 kHz.

MPPT algorithm is developed here is the P&O algorithm. Hybrid energy of wind and solar incorporates the duty cycle variation also. Sudden change in the wind and solar output power the dc bus voltage is preset, resulting in a change in the output current of the KY boost converter fed to the dc bus. A current sensor senses the current and compares it with the previous value. The duty ratio of the KY boost converter hence increases or decreases. Sensing wind speed and solar insolation by adjusting the duty ratio of the KY boost converter and continuously monitoring the parameters. In all-day shifts, the maximum power of the PV module and wind is extracted using the Maximum Power Point Tracking (MMPT) technique. To gain maximum power from both renewable energy the perturb and observe method is implemented.

To obtain maximum power operating voltage or current of the panel is modified. If the voltage to a cell increases the power of a cell, decreases. When the power output begins to decrease the corresponding operating voltage begins to decrease. Once this situation exists, the voltage is decreased to set back to the maximum power value. This procedure persists until the maximum power point is reached. Thus, the power value fluctuates around a maximum power value until it settles.

This algorithm mainly focused on operating voltage and the corresponding deviation of power is noted. If the difference in power is positive the future perturbation should follow the same to obtain MPP. If the deviation in power is negative the perturbation should be reversed and move reverse in direction to obtain MPP. This procedure continues until it achieves maximum power.

4.3 Controller

The voltage and frequency of MGs are strongly impressionable from the active and reactive load fluctuations. A change in load leads to an imbalance between generation and consumption. The output voltage and frequency of the DGs are primarily controlled by the droop characteristics. But, in case of severe changes in load, the DGs may be failed and the Microgrid is collapsed. Subsequently, the research proposed the interval type 3 fuzzy controller is used for controlling the load frequency of the multi-area system. A 1% step load perturbation is applied to the load demand of the power plant and analysis of the system responses in terms of settling time, peak overshoot and peak undershoot. Henceforth, it is necessary to maintain the system frequency to be constant. Consequently, the research proposed a swarm-based hybrid metaheuristic optimizer of the Bacterial Foraging Optimization Algorithm (BFOA) which optimally tunes and controls the PI controller parameters. However, most fuzzy controllers are static in that they respond only to current input, so they may not offer any improvement over the

dynamic nature of designs. By replacing nonlinear and time-varying aspects of a neural network with uncertainties, a robust reinforcement learning procedure results that are guaranteed to remain stable even as the neural network is being trained. The behaviour of this procedure is demonstrated and analyzed on two simple control tasks.

4.3.1 Interval Type 3 Fuzzy Controller

The interval type-3 FLSs (IT3-FLSs) are developed to handle more levels of uncertainty. In this study, IT3-FLSs are used for online dynamic identification. The structure of IT3-FLS is explained step-by-step below:

The inputs of IT3-FLSs are $y_1 = I_p(t)$, $y_2 = V_c(t-\tau)$, $y_3 = I_b(t)$, where, I_p and I_b are the currents of PV and battery, respectively and V_c is the load voltage. τ represents the sample time.

For each input, two Gaussian membership functions (MFs) are considered. The centres of MFs are set to the upper and lower bounds of each input. For input I_p, $\tilde{A}^2_{I_p}$, respectively. Similarly, for input I_b, one has: the upper and lower memberships are obtained as:

$$\bar{\mu}_{\tilde{A}^1_{I_p}|\alpha}(I_p) = exp\left(-\frac{\left(I_p - \underline{c}_{\tilde{A}^1_{I_p}}\right)^2}{\bar{\sigma}^2_{\tilde{A}^1_{I_p}|\alpha}}\right) \quad (5)$$

$$\bar{\mu}_{\tilde{A}^2_{I_p}|\alpha}(I_p) = exp\left(-\frac{\left(I_p - \bar{c}_{\tilde{A}^2_{I_p}}\right)^2}{\bar{\sigma}^2_{\tilde{A}^2_{I_p}|\alpha}}\right) \quad (6)$$

$$\underline{\mu}_{\tilde{A}^1_{I_p}|\alpha}(I_p) = exp\left(-\frac{\left(I_p - \underline{c}_{\tilde{A}^1_{I_p}}\right)^2}{\underline{\sigma}^2_{\tilde{A}^1_{I_p}|\alpha}}\right) \quad (7)$$

$$\underline{\mu}_{\tilde{A}^2_{I_p}|\alpha}(I_p) = exp\left(-\frac{\left(I_p - \bar{c}_{\tilde{A}^2_{I_p}}\right)^2}{\underline{\sigma}^2_{\tilde{A}^2_{I_p}|\alpha}}\right) \quad (8)$$

Where, α is the level of the horizontal slice. $\tilde{A}^1_{I_p}$ and $\tilde{A}^2_{I_p}$ are the first and second MFs for input I_p. $\underline{c}_{\tilde{A}^1_{I_p}}$ and $\bar{c}_{\tilde{A}^2_{I_p}}$ are the centres of $\tilde{A}^1_{I_p}$ and $\tilde{A}^2_{I_p}$, respectively. $\bar{\sigma}_{\tilde{A}^1_{I_p}|\alpha}$/ $\underline{\sigma}_{\tilde{A}^1_{I_p}|\alpha}$ and $\bar{\sigma}_{\tilde{A}^2_{I_p}|\alpha}/\underline{\sigma}_{\tilde{A}^2_{I_p}|\alpha}$ are the standard division for the upper/lower bounds of $\tilde{A}^1_{I_p}$ and $\tilde{A}^2_{I_p}$, respectively. Similarly, for input I_b, one has:

$$\bar{\mu}_{\tilde{A}^1_{I_b}|\alpha}(I_b) = exp\left(-\frac{\left(I_b - \underline{c}_{\tilde{A}^1_{I_b}}\right)^2}{\bar{\sigma}^2_{\tilde{A}^1_{I_b}|\alpha}}\right) \quad (9)$$

$$\bar{\mu}_{\tilde{A}^2_{I_b}|\alpha}(I_b) = exp\left(-\frac{\left(I_b - \bar{c}_{\tilde{A}^2_{I_b}}\right)^2}{\bar{\sigma}^2_{\tilde{A}^2_{I_b}|\alpha}}\right) \quad (10)$$

$$\underline{\mu}_{\tilde{A}^1_{I_b}|\alpha}(I_b) = exp\left(-\frac{\left(I_b - \underline{c}_{\tilde{A}^1_{I_b}}\right)^2}{\underline{\sigma}^2_{\tilde{A}^1_{I_b}|\alpha}}\right) \quad (11)$$

$$\underline{\mu}_{\tilde{A}^2_{I_b}|\alpha}(I_b) = exp\left(-\frac{\left(I_b - \bar{c}_{\tilde{A}^2_{I_b}}\right)^2}{\underline{\sigma}^2_{\tilde{A}^2_{I_b}|\alpha}}\right) \quad (12)$$

Where, $\tilde{A}^1_{I_b}$ and $\tilde{A}^2_{I_b}$ are the first and second MFs for input Ib. $\underline{c}_{\tilde{A}^1_{I_b}}$ and $\bar{c}_{\tilde{A}^2_{I_b}}$ are the centres of $\tilde{A}^1_{I_b}$ and $\tilde{A}^2_{I_b}$, respectively. $\bar{\sigma}_{\tilde{A}^1_{I_b}|\alpha}/\underline{\sigma}_{\tilde{A}^1_{I_p}|\alpha}$ and $\bar{\sigma}_{\tilde{A}^2_{I_b}|\alpha}/\underline{\sigma}_{\tilde{A}^2_{I_b}|\alpha}$ are the standard division for the upper/lower bounds of $\tilde{A}^1_{I_b}$ and $\tilde{A}^2_{I_b}$, respectively. Finally, for input V_c, one has:

$$\bar{\mu}_{\tilde{A}^1_{V_c}|\alpha}(V_c) = exp\left(-\frac{\left(V_c - \underline{c}_{\tilde{A}^1_{V_c}}\right)^2}{\bar{\sigma}^2_{\tilde{A}^1_{V_c}|\alpha}}\right) \quad (13)$$

$$\bar{\mu}_{\tilde{A}^2_{V_c}|\alpha}(V_c) = exp\left(-\frac{\left(V_c - \bar{c}_{\tilde{A}^2_{V_c}}\right)^2}{\bar{\sigma}^2_{\tilde{A}^2_{V_c}|\alpha}}\right) \quad (14)$$

$$\underline{\mu}_{\tilde{A}^1_{V_c}|\alpha}(V_c) = exp\left(-\frac{\left(V_C - \underline{c}_{\tilde{A}^1_{V_c}}\right)^2}{\underline{\sigma}^2_{\tilde{A}^1_{V_c}|\alpha}}\right) \quad (15)$$

$$\underline{\mu}_{\tilde{A}^2_{V_c}|\alpha}(V_c) = exp\left(-\frac{\left(V_c - \bar{c}_{\tilde{A}^2_{V_c}}\right)^2}{\underline{\sigma}^2_{\tilde{A}^2_{V_c}|\alpha}}\right) \quad (16)$$

Where, $\tilde{A}^1_{V_c}$ and $\tilde{A}^2_{V_c}$ are the first and second MFs for input V_c. $\underline{c}_{\tilde{A}^1_{V_c}}$ and $\bar{c}_{\tilde{A}^2_{V_c}}$ are the centres of $\tilde{A}^1_{V_c}$ and $\tilde{A}^2_{V_c}$, respectively. $\bar{\sigma}_{\tilde{A}^1_{V_c}|\alpha}/\underline{\sigma}_{\tilde{A}^1_{V_c}|\alpha}$ and $\bar{\sigma}_{\tilde{A}^2_{V_c}|\alpha}/\underline{\sigma}_{\tilde{A}^2_{V_c}|\alpha}$ are the standard division for the upper/lower bounds of $\tilde{A}^1_{V_c}$ and $\tilde{A}^2_{V_c}$, respectively. 3) The output of $\hat{f}_1$ and $\hat{f}_2$ are:

$$\hat{f}_1 = \theta_1^T \zeta_1 \quad (17)$$

$$\hat{f}_2 = \theta_2^T \zeta_2 \quad (18)$$

Where, θ_i and ζ_i are:

$$\theta_i = \left[\underline{w}_{i1}, \dots, \underline{w}_{iR}, \bar{w}_{i1}, \dots, \bar{w}_{iR}\right]^T \quad (19)$$

$$\zeta_i = \left[\underline{\zeta}_{i1}, \dots, \underline{\zeta}_{iR}, \bar{\zeta}_{i1}, \dots, \bar{\zeta}_{iR}\right]^T \quad (20)$$

Where, $\bar{w}_{i1}$ and $\underline{w}_{j1}$ are the parameters of $l-$th rule for $i-$th IT3-FLS and R represents the number of rules. $\underline{\zeta}_{i1}$ and $\bar{\zeta}_{i1}$ are:

$$\bar{\zeta}_l = \frac{\sum_{j=1}^{n_\alpha} \bar{\alpha}_j \frac{\bar{z}^l_{\mu s=\bar{\alpha}_j}}{\sum_{l=1}^{R}\left(\bar{z}^l_{\mu s=\bar{\alpha}_j} + \underline{z}^l_{\mu s=\bar{\alpha}_j}\right)}}{\sum_{j=1}^{n_\alpha}(\bar{\alpha}_j + \underline{\alpha}_j)} + \frac{\sum_{j=1}^{n_\alpha} \underline{\alpha}_j \frac{\bar{z}^l_{\mu s=\underline{\alpha}_j}}{\sum_{l=1}^{R}\left(\bar{z}^l_{\mu s=\underline{\alpha}_j} + \underline{z}^l_{\mu s=\underline{\alpha}_j}\right)}}{\sum_{j=1}^{n_\alpha}(\bar{\alpha}_j + \underline{\alpha}_j)}, \; l = 1, \dots 8 \quad (21)$$

$$\underline{\zeta}_l = \frac{\sum_{j=1}^{n_\alpha} \bar{\alpha}_j \frac{\underline{z}^l_{\mu s=\bar{\alpha}_j}}{\sum_{l=1}^{R}\left(\bar{z}^l_{\mu s=\bar{\alpha}_j} + \underline{z}^l_{\mu s=\bar{\alpha}_j}\right)}}{\sum_{j=1}^{n_\alpha}(\bar{\alpha}_j + \underline{\alpha}_j)} + \frac{\sum_{j=1}^{n_\alpha} \underline{\alpha}_j \frac{\underline{z}^l_{\mu s=\underline{\alpha}_j}}{\sum_{l=1}^{R}\left(\bar{z}^l_{\mu s=\underline{\alpha}_j} + \underline{z}^l_{\mu s=\underline{\alpha}_j}\right)}}{\sum_{j=1}^{n_\alpha}(\bar{\alpha}_j + \underline{\alpha}_j)}, \; l = 1, \dots 8 \quad (22)$$

Where, n_α is the number of horizontal slices and:

$$\underline{\zeta}_l = \frac{\sum_{j=1}^{n_\alpha} \bar{\alpha}_j \frac{\underline{z}^l_{\mu s=\bar{\alpha}_j}}{\sum_{l=1}^{R}\left(\bar{z}^l_{\mu s=\bar{\alpha}_j} + \underline{z}^l_{\mu s=\bar{\alpha}_j}\right)}}{\sum_{j=1}^{n_\alpha}(\bar{\alpha}_j + \underline{\alpha}_j)} + \frac{\sum_{j=1}^{n_\alpha} \underline{\alpha}_j \frac{\underline{z}^l_{\mu s=\underline{\alpha}_j}}{\sum_{l=1}^{R}\left(\bar{z}^l_{\mu s=\underline{\alpha}_j} + \underline{z}^l_{\mu s=\underline{\alpha}_j}\right)}}{\sum_{j=1}^{n_\alpha}(\bar{\alpha}_j + \underline{\alpha}_j)}, \; l = 1, \dots R \quad (23)$$

The rules are written as:

Rule #1: If I_p is $\tilde{A}^1_{I_p}|\alpha$ and I_b is $\tilde{A}^1_{I_b}|\alpha$ and V_c is $\tilde{A}^1_{V_c}|\alpha$

Then $\hat{f}_i \in [\underline{w}_{j1}, \bar{w}_{i1}]$

Rule #2: If I_p is $\tilde{A}^1_{I_p}|\alpha$ and I_b is $\tilde{A}^1_{I_b}|\alpha$ and V_c is $\tilde{A}^2_{V_c}|\alpha$

Then $\hat{f}_i \in [\underline{w}_{j2}, \bar{w}_{i2}]$

Rule #3: If I_p is $\tilde{A}^1_{I_p}|\alpha$ and I_b is $\tilde{A}^2_{I_b}|\alpha$ and V_c is $\tilde{A}^1_{V_c}|\alpha$

Then $\hat{f}_i \in [\underline{w}_{j3}, \bar{w}_{i3}]$

Rule #4: If I_p is $\tilde{A}^1_{I_p}|\alpha$ and I_b is $\tilde{A}^2_{I_b}|\alpha$ and V_c is $\tilde{A}^2_{V_c}|\alpha$

Then $\hat{f}_i \in [\underline{w}_{j4}, \bar{w}_{i4}]$

Rule #5: If I_p is $\tilde{A}^2_{I_p}|\alpha$ and I_b is $\tilde{A}^1_{I_b}|\alpha$ and V_c is $\tilde{A}^1_{V_c}|\alpha$

Then $\hat{f}_i \in [\underline{w}_{j5}, \bar{w}_{i5}]$

Rule #6: If I_p is $\tilde{A}^2_{I_p}|\alpha$ and I_b is $\tilde{A}^1_{I_b}|\alpha$ and V_c is $\tilde{A}^2_{V_c}|\alpha$

Then $\hat{f}_i \in [\underline{w}_{j6}, \bar{w}_{i6}]$

Rule #7: If I_p is $\tilde{A}^2_{I_p}|\alpha$ and I_b is $\tilde{A}^2_{I_b}|\alpha$ and V_c is $\tilde{A}^1_{V_c}|\alpha$

Then $\hat{f}_i \in [\underline{w}_{j7}, \bar{w}_{i7}]$

Rule #8: If I_p is $\tilde{A}^2_{I_p}|\alpha$ and I_b is $\tilde{A}^2_{I_b}|\alpha$ and V_c is $\tilde{A}^2_{V_c}|\alpha$

Then $\hat{f}_i \in [\underline{w}_{j8}, \bar{w}_{i8}]$

In the type-3 MFs, the secondary membership is not a crisp value but it is a fuzzy set. Also a horizontal slice of a level $\mu_s = \alpha_k$ is equal with two slices at levels $\mu_s = \underline{\alpha}_k$ and $\mu_s = \overline{\alpha}_k$ in type-2 counterpart.

4.3.2 Swarm-Based Hybrid Metaheuristic Optimizer

In BFOA, chemotaxis is the ground of the local search, and reproduction accelerates convergence speed. Elimination-dispersal loops avoid immature convergence and advance the search in the direction of the global maxima via elimination-dispersal loops. But chemotaxis and reproductions are insufficient to trace the global maxima as the bacteria may be trapped in local maxima as the dispersion occurs after several reproduction stages. In BFOA, there is a feasibility to avoid being stuck in local optima by incorporating mutation. The mutation leads to a diverse population to obviate the possibility of an immature convergence and simultaneously avoids being trapped in local maxima.

In BFOA, the run length in every generation has a key role in the occurrence and convergence to the global optimum value. Because of the fixed step size in BFOA, the algorithm bears mainly two problems:

If the run length is kept very small, then this leads to a rise in the generation count to reach the global maxima, i.e., the iterations required will be increased for getting the optimal solution. An increase in run length results in a faster convergence rate, i.e., the bacteria reach the global optima swiftly, but the accuracy is compromised.

In the proposed paper, a unique approach for the position update of bacteria is used to aggravate the convergence rate and precision of the algorithm. The first step includes the update in the bacteria position after evaluating the fitness value for the generation. In a later stage, the mutation with PSO parameters is introduced to tune the diversity in the bacterium position update. PSO parameters are independent parameters such as inertia, mass, weight, or accelerating coefficient for the best tuning to achieve the global optimum value. In the hybrid PSO-BFOA algorithm, any local search is performed using chemotaxis, whether the global search is accomplished using reproduction and mutation.

The role of the mutation operator is summarized as:

On the completion of the chemotaxis process, the bacterium positions are updated using mutation to reach the global maxima. The mutation performs a crucial part in the fine-tuning of the PSO-BFOA algorithm and simultaneously maintaining precision in achieving the optimal solution. Initially, the ratio of global θ and $\theta(i,j,k)$ becomes very less that results in a wide run length, but in a later stage, the run length is minimized as $\theta(i,j,k)$ is very close to the global θ. Because of the increase in the number of generations, the bacterium will be captivated towards the global optima. At this stage, $\theta(i,j,k)$ is updated as: $\theta(i,j+1,k) = \left(1 - \frac{\theta_{global}}{\theta(i,j,k)}\right) * r_1 * \theta_{global} + \left(\frac{\theta_{global}}{\theta(i,j,k)}\right) * r_2 * \theta_{pbest}(j,k)$. Where, θ is the bacterium position in the search space, i, j, and k stand for the number of bacteria, chemotaxis step, and reproduction step, respectively.

θ_{pbest} is the local optimal position, θ_{global} represents the global optimal position, and r_1, r_2 are the random variables.

The Hybrid PSO-BFOA algorithm is summarized as:

1. Initialization of the Parameters S, N_c, N_s, N_{re}.
2. Restore the following parameters

$$J_{best}(j,k) \tag{24}$$

$$J_{global} = J_{best}(j,k) \tag{25}$$

Where, j represents the fitness value, J_{best} and J_{global} stands for local and global fitness values, respectively

3. Reproduction loop: $k = k + 1$
4. Chemotaxis loop: $j = j + 1$

(a) Calculate the fitness value $J(i,j,k)$ for $i = 1,2,3 \ldots S$ and accordingly, restore $J_{best}(j,k)$ and $\theta_{pbest}(j,k)$

(b) Tumble: random vector generation $\Delta(i) \in R^p$ for every element

$\Delta m(i), m = 1,2,\ldots,p$, a random variable

(c) Evaluate θ for $i = 1, 2 \ldots S$

$$\theta(i, j+1 \cdot k) = \theta(i, j, k) + c(i) \frac{\Delta(i)}{\sqrt{\Delta^T(i)\Delta(i)}} \quad (26)$$

(d) Swim

(i) Let $m = 0$ (counter for swim length)

(ii) While $m < N_s$

Let $m = m + 1$

Evaluate the fitness function $J(i, j+1 \cdot k)$ for $i = 1, 2, 3 \ldots S$ Restore $J_{best}(j + 1, k)$

- If $J_{best}(j+1, k) < J_{best}(j, k)$ (if performing better) then $J_{best}(j, k) = J_{best}(j + 1, k)$ and $\theta_{pbest}(j, k) = \theta_{pbest}(j + 1, k)$

Use the equation for $\theta(i, j+1, k)$ to calculate the new $J(i, j+1, k)$.

- Else, let $m = N_s$.

(e) Mutation: Change the positions of the bacterium by mutation. Compare θ for $i = 1, 2 \ldots S$

$$\theta(i, j+1 \cdot k) = \left(1 - \frac{\theta_{global}}{\theta(i,j,k)}\right) * r_1 * \theta_{global} + \left(\frac{\theta_{global}}{\theta(i,j,k)}\right) * r_2 * \theta_{pbest}(j, k) \quad (27)$$

5. If $j < N_c$, jump to step 4 and continue chemotaxis, as the lives of the bacterium are not completed.

6. The $S_r = S/2$ bacteria with the optimum fitness value (J) dies and other S_r bacteria have the best value splits. Restore J_{global} and θ_{global}.

7. If $k < N_{re}$, go to step 3. Instead, stop.

The PSO Fitness estimation approach for solving complex computational problems has already been formulated. Standard PSO assumes that each particle possesses a certain position and velocity. Every position is a trial solution to the problem, which is optimized. The movement is determined by the velocity. Hence, the flying particle here is the swarm search of the domain. The velocity and position of a particle flying from its original position to a different position are updated using the relation:

$$\vec{v}_i(t+1) = \omega \vec{v}_i(t) + c_1 r_1 \left(\vec{p}_i(t) - \vec{x}_i(t)\right) + c_2 r_2 \left(\vec{p}_g(t) - \vec{x}_i(t)\right) \quad (28)$$

$$\vec{x}_i(t+1) = \vec{x}_i(t) + \vec{v}_i(t+1) \quad (29)$$

Where, $\vec{v}_i(t)$ and $\vec{x}_i(t)$ are the ith particles velocity and position at tth iteration; $\vec{p}_i(t)$ and $\vec{p}_g(t)$ represents the ith particle's optimal position observed so far and the globally observed optimal position of all the particles up to iteration t. ω reflects the inertia weight; c_1, c_2 stands for cognitive and social parameters. r_1, r_2 are diagonal matrices, where the diagonal entries lie in the range of $(0, 1)$.

Since in the proposed hybrid metaheuristic optimizer, PSOBFOA, the mutation with PSO parameters helps to trace the global optima; hence the fitness estimation approach of the proposed hybrid PSO-BFOA optimizer is considered similar to that of the PSO optimizer.

4.4 System Stability with Penetration Level Evaluation

Power system stability is an important area of concern in modern interconnected power systems. It is termed as the capability of a power system to become stable after the removal of disturbances. While an unstable system loses its control by falling out of synchronism, this phenomenon may have a catastrophic impact on the smooth running of the power system. In this study, a new reactive power control strategy is employed for optimization of the reactive power along with the stability improvement of the system under different small perturbed conditions. Therefore, this study focuses on controlling the reactive power of the hybrid power system model with the aid of a Static Synchronous Compensator (STATCOM). Further, evaluate the renewable energy resources' penetration limit of the AC-DC hybrid grid, which considers both economy and safety. The static stability indicators are

considered for an evaluation of the penetration limit of RES.

4.4.1 Static Synchronous Compensator

STATCOM is developed on the solid-state-based synchronous source of voltage which replicates a synchronous machine of ideal nature. It generates a set of 3-phase balanced sinusoidal voltages at the fundamental frequency by continuous controlling of phase angle and amplitude. The schematic of the STATCOM and its equivalent structure has been given in figure 3. Figure 3 illustrates the voltage source converter, DC capacitor, and coupling transformer. The real part of the STATCOM controller current is insignificant and considered zero. The reactive current can be controlled by the variation of α and δ.

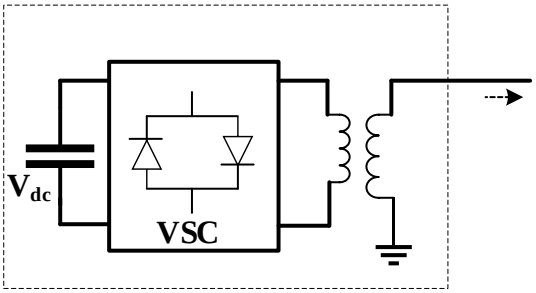

Figure 3: Schematic Diagram for STATCOM Configuration

In this paper, α is the STATCOM's fundamental output voltage (kV_{dc}) phase angle and δ is the phase angle of the system bus voltage, U where the STATCOM is connected. The amplitude of the converter's fundamental output voltage is $kU_{dc}$where U_{dc}represents DC voltage developed in between the DC capacitor. The STATCOM controller injecting the reactive power to the connected bus has been given as in equation (30).

$$Q_{STATCOM} = kU_{dc}^2 B - kU_{dc} UB\ cos\ (\alpha - \delta) + kU_{dc} UG\ sin(\alpha - \delta) \quad (30)$$

In the considered HPS, bus voltage is taken as a reference voltage; so, the bus angle (δ) is zero. In the above equation, the G term is also insignificant, because ($G + jB$) characterizes the admittance of the step-down transformer. Thus, equation (30) now becomes equation (31), considering G and δ as zero.

$$Q_{STATCOM} = kU_{dc}^2 B - kU_{dc} UB\ cos\alpha \quad (31)$$

Here, in equation (31), U and α, are the variable terms on which the reactive power depends; under the small perturbations, the change in reactive power of STATCOM can be written as equation (32).

$$\Delta Q_{STATCOM}\ (s) = G_1 \Delta\alpha(s) + G_2 \Delta U(s) \quad (32)$$

Where, $G_1 = kU_{dc} UB\ sin\alpha$ and $G_2 = kU_{dc} UB\ cos\alpha$.

It evaluates the renewable energy resources' penetration limit of the AC-DC hybrid grid, which considers both economy and safety. The static stability indicators are considered for an evaluation of the penetration limit of RES.

5. Experimentation and Result Discussion

The HMG is simulated using the Matlab/Simulink software to evaluate the performance of the proposed hybrid power system employed on the modified ILC. This evaluation consists of the power flow analyses and power quality factors at the DC-link of the DCMG, and at the utility grid. The loads and sources are rated up to 4.5 kW. The interlinking converters are designed for 3 kW of nominal power, which allows an adequate hybrid power system operation. The inductors and capacitors are

designed considering the power converters' voltage ripple and nominal power.

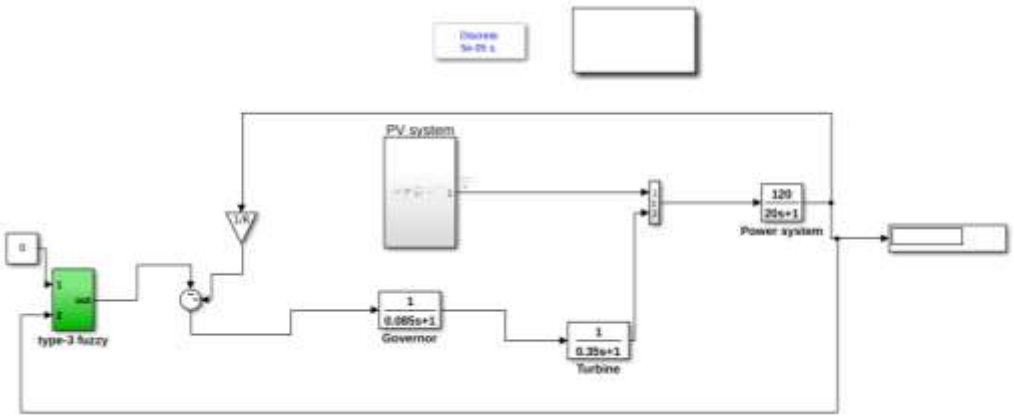

Figure 4: Simulation Model for Hybrid Renewable Energy Resources

The simulation model for hybrid renewable energy resources is presented in figure 4, which was done in MATLAB/SIMULINK environment. In Hybrid PV System, the PV system acts as a main source. Renewable energy resources are connected in parallel and the across this parallel combination, more than 30 V battery is connected which is in charging mode. If the voltage across this parallel combination is less than 30 V, the battery is in discharging mode. If the battery is only present in the circuit, the percentage semi-oxide concentration linearly decreases and battery voltage rapidly decreases. The main blocks in the above Simulink diagram are the PV model block, type 3 fuzzy model, governor, turbine, MPPT block, DC/DC converter block, Battery model and power system. The optimum power control and pitch angle control act as prime movers for the induction generator. The external inputs to the turbine are wind speed and rotor speed. The grid side converter's main objective is to regulate the DC link capacitor voltage and this converter controls the power flow between the DC bus and the AC side.

Table 1: Simulation System Configuration

Simulation System Configuration	
MATLAB Simulink	Version R2021a
Operation System	Windows 10 Home
Memory Capacity	6GB DDR3
Processor	Intel Core i5 @ 3.5GHz
Simulation Time	10.190 seconds

The simulation system configuration of the proposed work is portrayed in table 1. Subsequently, the proposed technique is evaluated and tested under the Matlab R2021a software. The proposed work operates under windows 10 home and its memory capacity is 6GB DDR3. Additionally, it utilizes an Intel Core i5 @ 3.5GHz processor and the simulation time of the work is 10.190 seconds.

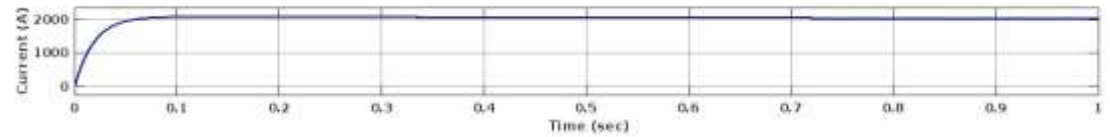

(a) Current

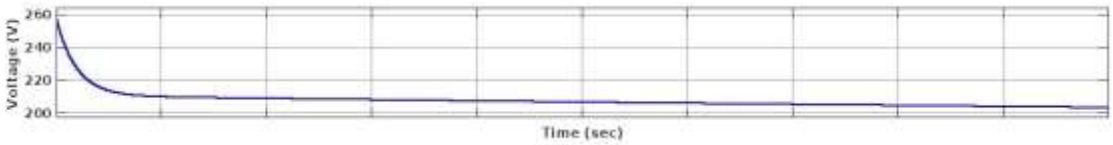

(b) Voltage

Figure 5: Current and Voltage Graph for Battery

The current and voltage graph for the battery is presented in figure 5. It produces a battery current of approximately 2000 A for 1 second. However, the voltage produced due to the battery is approximately 205 V for time 1 second. The input charging current to the battery stack in a photovoltaic hybrid solution will not be constant due to the atmospheric conditions and the time of day.

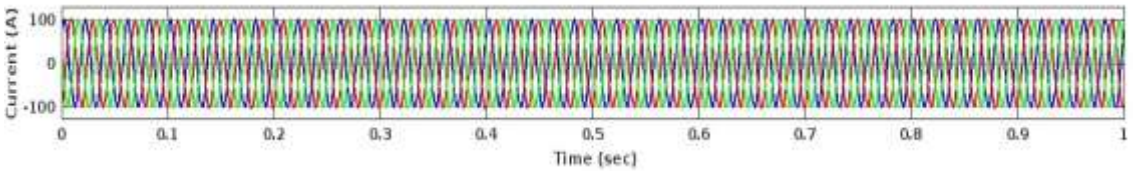

(a) Current

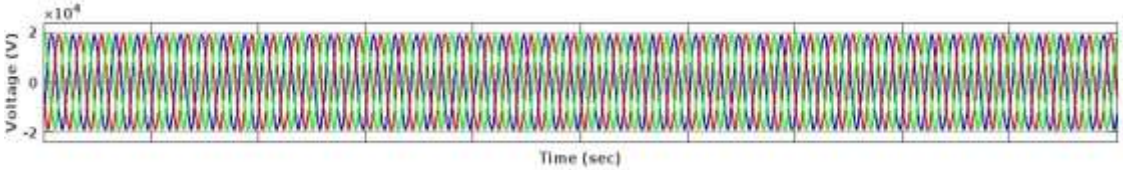

(b) Voltage

Figure 6: Grid Current and Grid Voltage

Figure 6 reveals the grid current and grid voltage. The grid current is regulated to its nominal value and is in phase with the grid voltage as can be seen in figure 9. It shows the high quality of the current injected into the grid with the proposed current control scheme. This result meets the requirements of the grid-connection standard. The grid voltage produces 1.9×10^4v. The grid voltage harmonic disturbances are rejected by the robust ADRC controller, leading to much better performance.

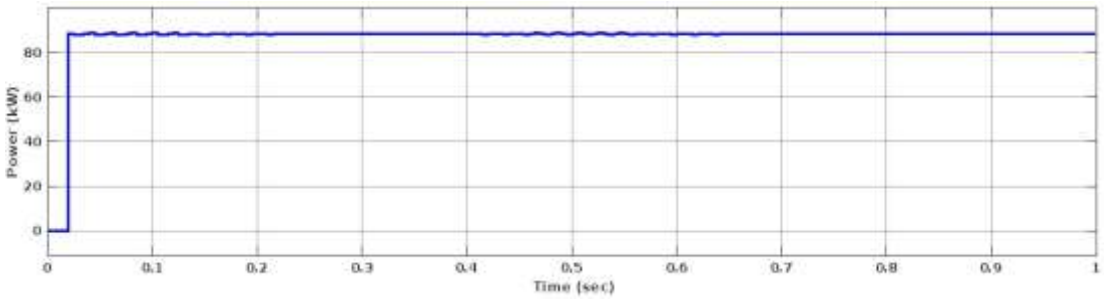

Figure 7: Power for HMG

The power graph for the proposed hybrid power system is presented in figure 7. It produces approximately 90 kW of power generated from hybrid power systems. This power value is measured based on the time seconds. This reading of power was measured when the time was 0 to 1 second, respectively.

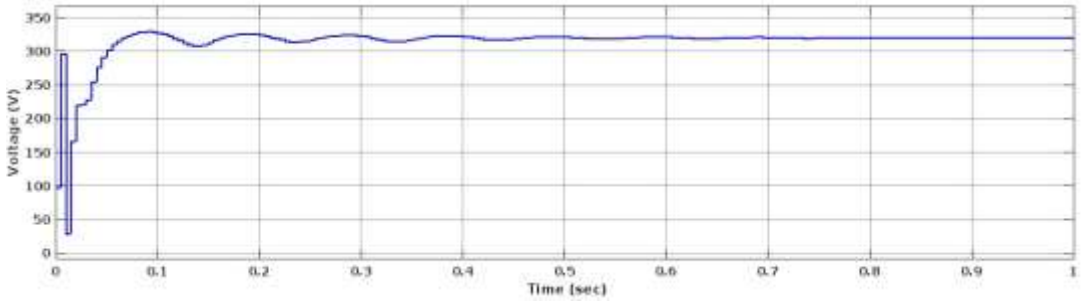

(a) Voltage for PV Panel

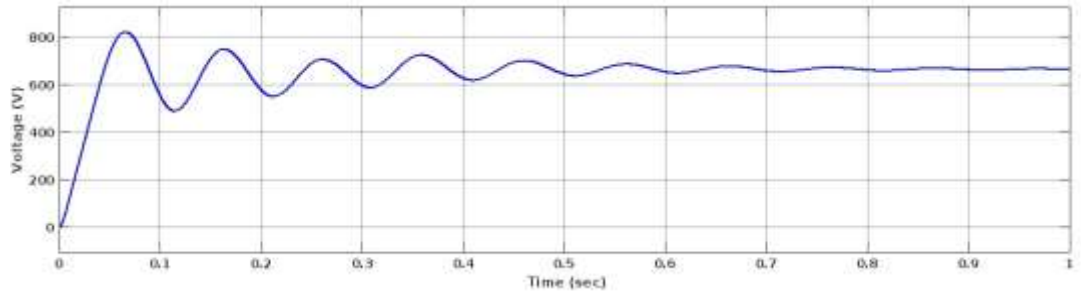

(b) Voltage for VDC

Figure 8: Output Voltage Graph

Figure 8 (a) represents the PV panel of output voltage. By using an array combination the maximum output voltage is =325 volts (65 *5). The PV panel maintains the constant DC voltage (325 volts) shown in this figure. However, figure (b) portrays the voltage of the Vdc graph, which produces a voltage of 670 v for the time of 1 second. But the maximum voltage produced is 820 v, respectively.

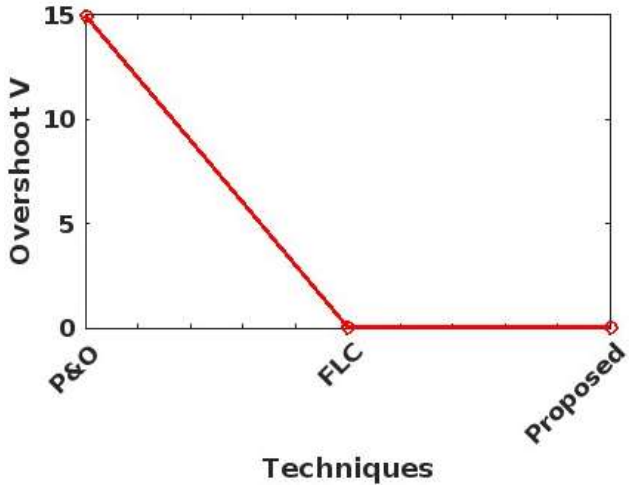

Figure 9: Comparison Graph for Overshoot Voltage

Figure 9 depicts the comparison graph for the overshoot voltage of converters. It shows the output voltage waveforms with an overshoot of different converters' performance like P&O, FLC, and proposed converter. The maximum allowed variation for the output voltage during load transient is calculated in this figure. These perturbations are limited by the joint action of the output capacitor and the feedback control: the former limits the initial overshoot caused by a sudden change in load current, whereas the controller behaviour depends on the control circuit being used. From this figure, the existing P&O method is unstable, and the FLC is stable but the proposed method is more stable than these existing techniques.

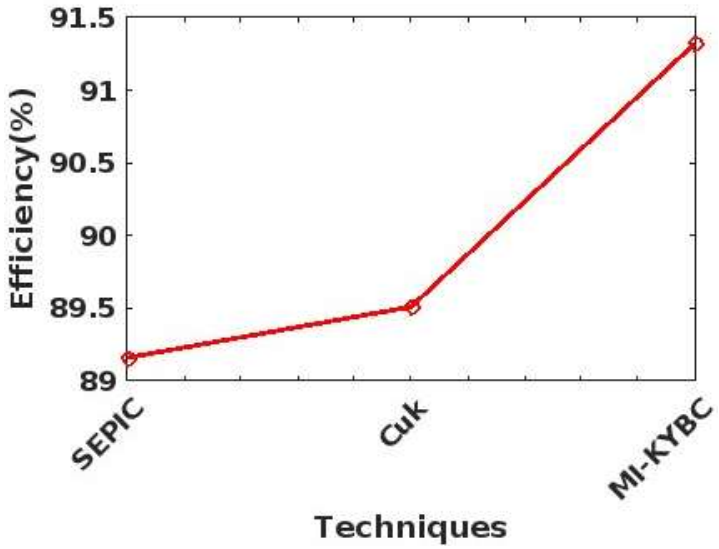

Figure 10: Comparison Graph for Efficiency of the Converters

The efficiency graph for the proposed method is compared with the existing SEPIC and Cuk converters and is presented in figure 10. While compare to these existing converters, the proposed converters produce higher efficiency that is the efficiency of the proposed technique is 91.3%, but the other existing converters SEPIC and Cuk produce lower efficiency values of 89.16 and 89.51, respectively,

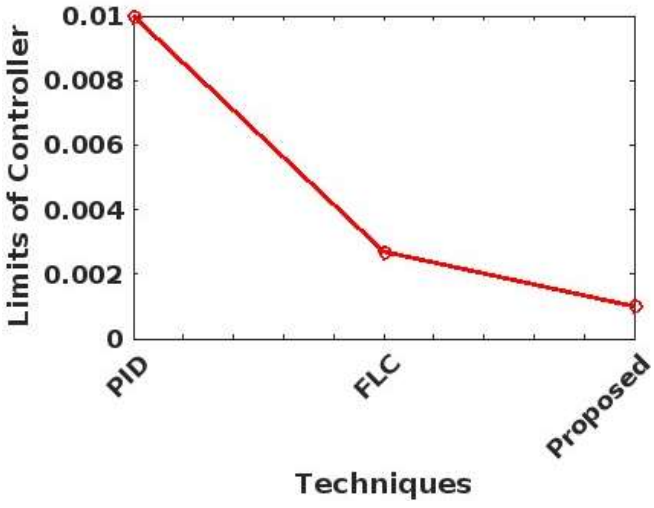

Figure 11: Comparison Graph for Limits of Controller

The limits of the controller compared to the existing PID and FLC controllers are presented in this figure 11. The figure depicts that the limits of the PID controller are 0.01, and the limits of FLC controllers are 0.0027, however, the proposed method produces lower controller limits of 0.0013, respectively.

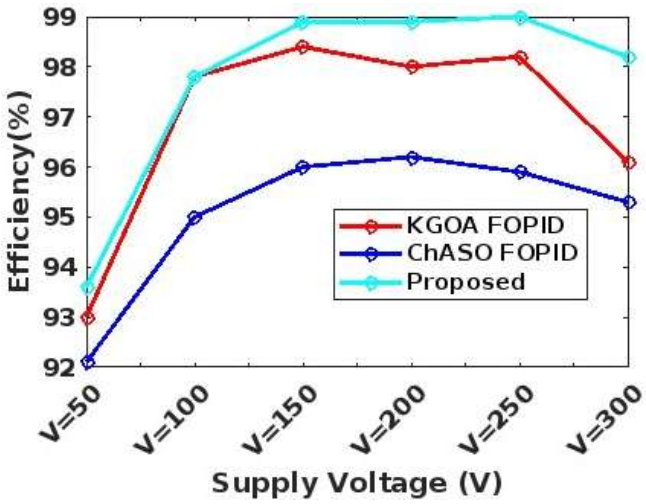

Figure 12: Efficiency Graph for Controllers

Figure 12 reveals the comparison graph for the controllers' efficiency graph. The proposed efficiency is compared with the existing KGOA FOPID and ChASO FOPID controllers. The efficiency is evaluated based on the supply voltage from 50V to 300V. This figure depicted that the proposed method produces higher efficiency values of 98.2%.

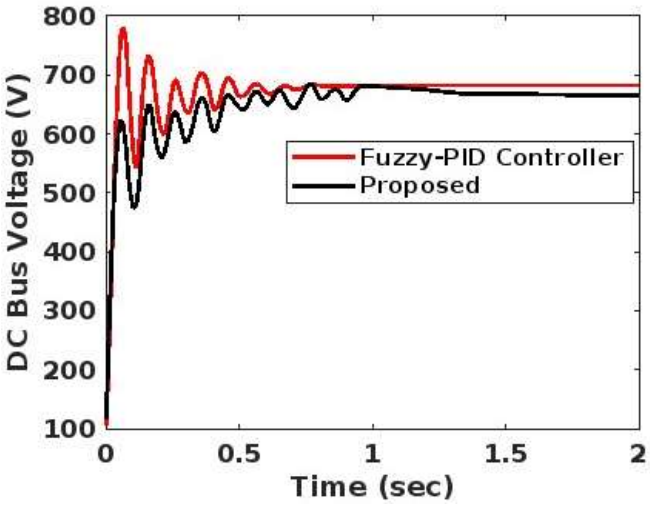

Figure 13: Comparison of DC Bus Voltage

Figure 13 reveals the comparison graph for DC bus voltages, the proposed IT3-FLS controller is compared with the existing Fuzzy-PID controller. It can be observed that the error signal contains only the DC component due to the cancellation of the ripple component in the measured DC bus

voltage. Consequently, the line current waveform is nearly sinusoidal.

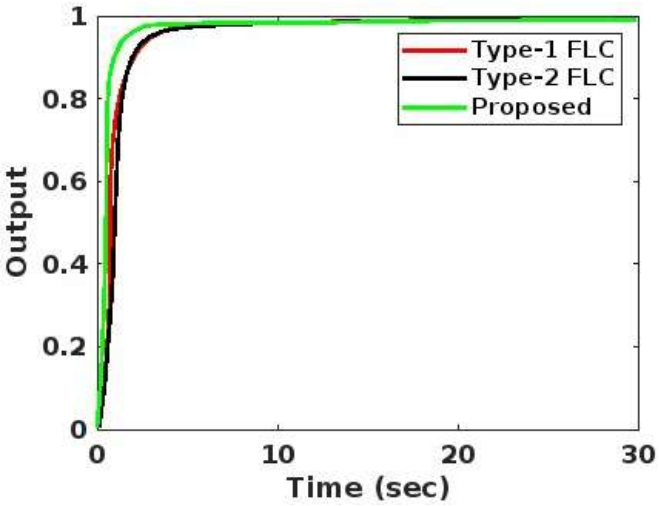

Figure 14: Comparison Graph for Dynamic Response of Controllers

Figure 14 reveals the comparison graph of the dynamic response of different controllers. The proposed Interval Type-3 FLC is compared with the existing methods like Type-1 FLC, and Type-2 FLC. It evaluates the proposed method and knows the dynamic performance of the control system. From this figure, the proposed method produces higher output dynamic response.

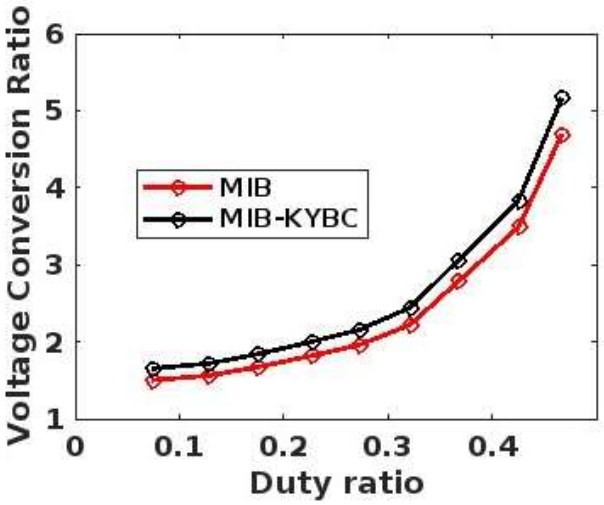

Figure 15: Comparison Graph for Voltage Conversion Ratio

Figure 15 portrays the comparison graph for the voltage conversion ratio, the proposed MIB-KYBC converter is compared with the existing MIB converter. The proposed converter has the voltage conversion ratio among these converters under different duty cycles, it can be seen that the proposed step-up converter possesses the highest voltage conversion ratio. The voltage conversion ratio of the proposed MIB-KYBC converter is up to 47.5 at the duty cycle is 0.47, respectively.

6. Research Conclusion

A microgrid is a small-scale electrical system composed of distributed generation (DG) and energy storage devices (ESD) technologies, with the aiming to meet the demand of local loads. In this work, a Multi-Input (MI) KY boost converter and type-3 fuzzy controller are proposed, Where, Swarm-based hybrid metaheuristic optimizer of the Bacterial Foraging Optimization Algorithm (BFOA) is proposed for optimally tuning and controlling the PI controller parameters. Controlling the reactive power of the hybrid power system model with the aid of a Static Synchronous Compensator (STATCOM). A hybrid microgrid comprising solar, battery, utility grid, and AC and DC loads is developed with ac and dc bus in MATLAB Simulink environment. The results demonstrate the superior performance of the proposed strategy based on the algorithm compared to the adaptive PI (API) controller in terms of fast response and tight regulation of power flow, voltage and frequency under different conditions. Compared to API, it has been found that the proposed controller results in more improvement of the dc-side voltage within the operating frequency range of the ac-side of the ILC. Accordingly, the penetration levels parameters are compared with the converter and the proposed control technique is to find the efficiency of the hybrid power system. The grid voltage produces 1.9×10^4v, the battery current produces approximately 2000 A for 1 second, and the voltage produced due to the battery is approximately 205 V for time 1 second. However, the obtained power-sharing reduces the energy supplied by the power grid, thereby avoiding concentrating the demanded effort in the battery system. The power quality analysis verified the effectiveness of the interlinking converters by mitigating harmonic distortions and reactive power for all the established operation conditions. In addition, it was noted the satisfactory performance of the voltage regulation, achieved by a hierarchical control, and applied to correct the voltage deviation caused by the droop technique. These results showed the capacity of the proposed modified interlinking converters to manage the power flow at all hybrid microgrid operating conditions, besides providing the desired ancillary services. In future, studies deep uncertainty study and stability analysis are presented, consequently, also presented the development of an intelligent control algorithm for the control of the HMG, respectively.

References

[1] Mosaad, M.I., Ramadan, H.S.M., Aljohani, M., El-Naggar, M.F. and Ghoneim, S.S., 2021. Near-optimal PI controllers of STATCOM for efficient hybrid renewable power system. IEEE Access, 9, pp.34119-34130.

[2] Munisamy, V. and Sundarajan, R.S., 2021. Hybrid technique for load frequency control of renewable energy sources with unified power flow controller and energy storage integration. International Journal of Energy Research, 45(12), pp.17834-17857.

[3] Samy, M.M., Elkhouly, H.I. and Barakat, S., 2021. Multi- objective optimization of hybrid renewable energy system based on biomass and fuel cells. International Journal of energy research, 45(6), pp.8214-8230.

[4] Razmjooy, N., Estrela, V.V., Padilha, R. and Monteiro, A.C.B., 2021. World cup optimization algorithm: Application for optimal control of pitch angle in hybrid renewable PV/wind energy system. In Metaheuristics and Optimization in Computer and Electrical Engineering (pp. 25-47). Springer, Cham.

[5] Elnozahy, A., Yousef, A.M., Abo-Elyousr, F.K., Mohamed, M. and Abdelwahab, S.A.M., 2021. Performance improvement of hybrid renewable energy sources connected to the grid using artificial neural network and sliding mode

control. Journal of Power Electronics, 21(8), pp.1166-1179.

[6] Ramesh, M., Yadav, A.K. and Pathak, P.K., 2021. An extensive review on load frequency control of solar-wind based hybrid renewable energy systems. Energy Sources, Part A: Recovery, Utilization, and Environmental Effects, pp.1-25.

[7] Mahto, T., Malik, H., Mukherjee, V., Alotaibi, M.A. and Almutairi, A., 2021. Renewable generation based hybrid power system control using fractional order-fuzzy controller. Energy Reports, 7, pp.641-653.

[8] Zangeneh, M., Aghajari, E. and Forouzanfar, M., 2022. Design and implementation of an intelligent multi-input multi-output Sugeno fuzzy logic controller for managing energy resources in a hybrid renewable energy power system based on Arduino boards. Soft Computing, 26(3), pp.1459-1473.

[9] Mudi, J., Shiva, C.K., Vedik, B. and Mukherjee, V., 2021. Frequency stabilization of solar thermal-photovoltaic hybrid renewable power generation using energy storage devices. Iranian Journal of Science and Technology, Transactions of Electrical Engineering, 45(2), pp.597-617.

[10] Mahmoudi, S.M., Maleki, A. and Ochbelagh, D.R., 2021. Optimization of a hybrid energy system with/without considering backup system by a new technique based on fuzzy logic controller. Energy Conversion and Management, 229, p.113723.

[11] Kumar, G.B., 2022. Optimal power point tracking of solar and wind energy in a hybrid wind-solar energy system. International Journal of Energy and Environmental Engineering, 13(1), pp.77-103.

[12] Chatterjee, S., Alam, A. and Ghose, T., 2021. Evaluation of the Performance of Droop Control Scheme for Interlinking Converter in Stand-Alone Hybrid Microgrid. In Advances in Smart Grid Automation and Industry 4.0 (pp. 807-816). Springer, Singapore.

[13] Angalaeswari, S., Jamuna, K., Natrayan, L., Ramesh, L. and Ramaswamy, K., 2022. Power-Sharing Analysis of Hybrid Microgrid Using Iterative Learning Controller (ILC) considering Source and Load Variation. Mathematical Problems in Engineering, 2022.

[14] Tafavogh, M. and Zahedi, A., 2021. Design and production of a novel encapsulated nano phase change materials to improve thermal efficiency of a quintuple renewable geothermal/hydro/biomass/solar/wind hybrid system. Renewable Energy, 169, pp.358-378.

[15] Sharma, M., Saxena, S., Prakash, S., Dhundhara, S. and Arya, Y., 2022. Frequency stabilization in sustainable energy sources integrated power systems using novel cascade noninteger fuzzy controller. Energy Sources, Part A: Recovery, Utilization, and Environmental Effects, 44(3), pp.6213-6235.

[16] Ahmed, M., Magdy, G., Khamies, M. and Kamel, S., 2022. An efficient coordinated strategy for frequency stability in hybrid power systems with renewables considering interline power flow controller and redox flow battery. Journal of Energy Storage, 52, p.104835.

[17] Dei, G., Gupta, D.K., Sahu, B.K., Jha, A.V., Appasani, B., Zawbaa, H.M. and Kamel, S., 2022. Improved Squirrel Search Algorithm Driven Cascaded 2DOF-PID-FOI Controller for Load Frequency Control of Renewable Energy Based Hybrid Power System. IEEE Access, 10, pp.46372-46391.

[18] Kumar, A., Gupta, D.K. and Ghatak, S.R., 2022, January. Fractional order PI Controller based Load Frequency Control of Hybrid Power System with Electric Vehicle. In 2022 2nd International Conference on Power

Electronics & IoT Applications in Renewable Energy and its Control (PARC) (pp. 1-6). IEEE.

[19] Sharma, M., Saxena, S., Prakash, S., Dhundhara, S. and Arya, Y., 2022. Frequency stabilization in sustainable energy sources integrated power systems using novel cascade noninteger fuzzy controller. Energy Sources, Part A: Recovery, Utilization, and Environmental Effects, 44(3), pp.6213-6235.

[20] Eluri, H. and Naik, M.G., 2022. Energy Management System and Enhancement of Power Quality with Grid Integrated Micro-Grid using Fuzzy Logic Controller. IJEER, 10(2), pp.256-263.

[21] Sundararaju, N., Vinayagam, A., Veerasamy, V. and Subramaniam, G., 2022. A Chaotic Search-Based Hybrid Optimization Technique for Automatic Load Frequency Control of a Renewable Energy Integrated Power System. Sustainability, 14(9), p.5668.

[22] Kumar, A. and Suhag, S., 2022. Whale optimization algorithm optimized fuzzy-pid plus pid hybrid controller for frequency regulation in hybrid power system. Journal of The Institution of Engineers (India): Series B, 103(2), pp.633-648.

[23] Aryan Nezhad, M., 2022. Frequency Control and Power Balancing in a Hybrid Renewable Energy System (HRES): Effective Tuning of PI Controllers in the Secondary Control Level. Journal of Solar Energy Research, 7(1), pp.963-970.

[24] Zhang, Y., Cheng, C., Cai, H., Jin, X., Jia, Z., Wu, X., Su, H. and Yang, T., 2022. Long-term stochastic model predictive control and efficiency assessment for hydro-wind-solar renewable energy supply system. Applied Energy, 316, p.119134.

[25] Chitra, L. and Kavitha Kumari, K.S., 2022. Artificial Intelligent Based Control of Improved Converter for Hybrid Renewable Energy Systems. In Proceedings of International Joint Conference on Advances in Computational Intelligence (pp. 583-596). Springer, Singapore.

Contribution of Individual Authors to the Creation of a Scientific Article (Ghostwriting Policy)

The authors equally contributed in the present research, at all stages from the formulation of the problem to the final findings and solution.

Sources of Funding for Research Presented in a Scientific Article or Scientific Article Itself

No funding was received for conducting this study.

Conflict of Interest

The authors have no conflicts of interest to declare that are relevant to the content of this article.